Journal of Archaeological Science 96 (2018) 45–56

Contents lists available at ScienceDirect

Journal of Archaeological Science

journal homepage: www.elsevier.com/locate/jas

Bacterial tetraether lipids in ancient bones record past climate conditions at the time of disposal

James T. Dillon[a], Sam Lash[a,b,c], Jiaju Zhao[d], Kevin P. Smith[e], Peter van Dommelen[b,c,f], Andrew K. Scherer[f], Yongsong Huang[a,c,*]

[a] Department of Earth, Environmental and Planetary Sciences, Brown University, Providence, RI, United States
[b] Joukowsky Institute for Archaeology and the Ancient World, Brown University, Providence, RI, United States
[c] Institute at Brown for Environment and Society, Brown University, Providence, RI, United States
[d] Institute of Earth Environment, Chinese Academy of Sciences, Xian, Shanxi Province, PR China
[e] Haffenreffer Museum of Anthropology, Brown University, Providence, RI, United States
[f] Department of Anthropology, Brown University, Providence, RI, United States

ARTICLE INFO

Keywords:
Bone
Branched glycerol dialkyl glycerol tetraether
Paleoclimate
Archaeology

ABSTRACT

Assessing impacts of climate change on ancient human societies requires accurate reconstructions of regional climate variations. However, due to the scarcity of *in situ* climate indicators in archaeological sites, climate interpretation often relies on indirect, geographically distant data from geological archives such as lake or ocean sediments, ice cores and speleothems. Because many cultural changes occurred abruptly over periods of years to decades, and are regional or even local in scale, correlating societal changes with climate reconstructions from geological archives induces significant uncertainties: factors such as chronological dating inconsistencies and geographic heterogeneity of climate can severely undermine interpretation. Here we show, for the first time, that it is possible to determine past climate change by analyzing bacteria-derived 'branched glycerol dialkyl glycerol tetraethers' (br-GDGTs) in ancient bones from archaeological sites. To the best of our knowledge this proxy has never been applied before to bones, nor with the intention of developing the method for application in archaeological research. We demonstrate that these compounds are likely derived from bacterial growth within bones following deposition in the ground, and the potential for their distributions to reflect climate and environmental conditions during the years immediately following deposition when bacteria consume internal substrates. Our preliminary results show that bone samples from different climate zones display distinct br-GDGT distributions. Well-dated late Pleistocene and Holocene bones from Alaska yield reconstructed temperatures consistent with existing climate reconstructions. While further work is necessary to determine how quickly the signal stabilizes in the bones, and to continue ongoing refinement of calibrations for temperature, precipitation, and other influences on br-GDGTs, we propose that br-GDGTs from ancient bones in archaeological sites may be taken as a new, *in situ* archive for reconstructing past climate conditions. This opens new perspectives for assessing connections between climate variations and social transformations in the past.

1. Introduction

Climate change has frequently been proposed as a key factor driving social change in ancient human societies. The socio-political collapse of the Classic-period Maya (Haug et al., 2003; Hodell et al., 1995; Kennett et al., 2012) and the transition of Chinese dynasties (Yancheva et al., 2007; Zhang et al., 2008) have for instance been attributed to major deficits of or abrupt changes in rainfall that fomented widespread famine, social unrest, violence and even warfare. The disappearance of Greenland's Norse colonies has been related to abrupt temperature declines during the Little Ice Age (D'Andrea et al., 2011). Evolution of bipedalism in hominins has also been related to forest contraction and grassland expansion as a result of reduced precipitation in East Africa (Potts, 1998).

In these instances, the evidence for climate change is derived from paleoclimate archives such as sediments, speleothems, and ice cores. While they undoubtedly provide key insights to climate variability, evidence from these sources is hampered by two important complications: (a) the challenge of accurately dating geological archives, and/or (b) the geographic heterogeneity of climate change at regional and

* Corresponding author. Department of Earth, Environmental and Planetary Sciences, Brown University, Providence, RI, United States.
E-mail address: yongsong_huang@brown.edu (Y. Huang).

https://doi.org/10.1016/j.jas.2018.05.009
Received 3 July 2017; Received in revised form 21 March 2018; Accepted 23 May 2018

continental scales. Errors associated with radiocarbon dates of sedimentary records can reach hundreds or even thousands of years, making it difficult to precisely correlate climate reconstructions to cultural events that have been dated separately using archaeological or radiometric methods that have their own dating imprecisions, albeit generally smaller. Social changes may occur over relatively short periods of time of just a few decades or less, which are brief enough to be lost in the variations of most techniques used to date geological archives and archaeological events. Correlating archaeological evidence of social change to proxy climate records is therefore extremely challenging.

Even if dating is accurate, as may often be the case for speleothem-based reconstructions, correlating climate change as recorded at the site of the climate proxy with the specific region where social change is observed from archaeological excavations still assumes uniformity of broader regional climate variations. Continental climate is however well known to be geographically highly variable, and proxy data from a single or limited number of locations are unlikely to offer a solid basis for extrapolating broad climate patterns for any given region. The speleothem evidence for climate change in the Maya lowlands is, for instance, derived from only a handful of places in Belize and the northwestern Yucatan Peninsula (Kennett et al., 2012; Medina-Elizalde et al., 2010; Webster et al., 2007), yet modern annual rainfall in the southern lowlands, which saw the Classic period collapse, varies quite dramatically, ranging from 1000 mm in the east (western Honduras) to 3000 mm in the west (Chiapas) (Scherer and Golden, 2014).

Ideally, climate proxies should be obtained directly from archaeological sites so that evidence of climate and social change can be traced in tandem, without the need for temporal or spatial extrapolation. Unfortunately, most archaeological sites do not possess the necessary climate proxies, whereas material culture collected and documented by archaeologists such as stone tools, architectural features or ceramics are not normally suitable for providing independent climate information.

Recent discovery of a class of ubiquitous bacterial lipids called branched GDGTs (br-GDGTs) in soils (Sinninghe Damsté et al., 2000; Weijers et al., 2006a) may, however, offer an opportunity to reconstruct climate conditions using material from archaeological sites. These lipids have been shown to vary systematically in structure with temperature and soil pH change across large gradients over the globe (De Jonge et al., 2014; Naafs et al., 2017; Peterse et al., 2012; Weijers et al., 2007a, 2006b). They are highly stable and can preserve past climate information over geological time scales (Gao et al., 2012; Peterse et al., 2011; Weijers et al., 2007b), and are thought to be produced by heterotrophic acidobacteria yet to be isolated (Weijers et al., 2006b; Sinninghe Damsté, 2016). The basis for geological and archaeological applications of GDGTs as chemical biomarkers is the assumption that variation in climatic variables, including mean annual air temperature (MAAT), soil pH, and precipitation, are reflected in the composition and distribution of these compounds, where GDGTs can vary in the number of methyl branches and the number of cyclopentane moieties (Sinninghe Damsté et al., 2000; Weijers et al., 2006b; Dang et al., 2016). Two global soil surveys, including 134 archive soils (Weijers et al., 2007a) and an expanded survey of 278 soils (Peterse et al., 2012), illustrate that the distribution of different GDGTs is correlated with climatic and environmental conditions, predominately mean annual air temperature (MAAT) and soil pH. The number of methyl branches was found to be closely related to MAAT and to a lesser extent to soil pH, while the number of cyclopentane moieties is related to soil pH (Weijers et al., 2007a). Cyclisation of Branch Tetraethers (CBT) and Methylation of Branched Tetraethers (MBT) indices were developed to quantify these changes. These indexes can then be expressed as functions of soil pH and MAAT based on GDGT distributions in global soil calibration datasets.

In practice, there may be additional factors influencing the relationship between the environmental variables (e.g., temperature or pH) and abundances of GDGTs. This has been reflected in relatively larger errors of the MBT-CBT paleotemperature proxy. However, natural soil samples with known temperature and pH gradients have illustrated the general reliability and potential of MBT-CBT-derived indices calculated using GDGT distributions, as well as the need to refine the calibration function (Peterse et al., 2012). The MBT-CBT proxy and its derivatives have been successfully used to infer past changes in continental temperature and pH from ocean margin sediments (Hopmans et al., 2004; Schouten et al., 2007; Weijers et al., 2007b), lake sediments (Blaga et al., 2010; Loomis et al., 2012; Tierney et al., 2012; Wu et al., 2013; Shanahan et al., 2013), paleosols and loess-paleosol sequences (Gao et al., 2012; Peterse et al., 2012; Yang et al., 2014); and peats (Zheng et al., 2015).

Faunal remains such as bones, whether from wild or domestic animals, are routinely encountered in substantial numbers at archaeological sites. The organic components of bone may offer excellent substrates for br-GDGT-producing heterotrophic bacteria, and if consumed relatively quickly, the resulting br-GDGTs inside bones would capture a snap-shot of the climate conditions soon after the bones' disposal. The physical structures of bone are moreover likely to isolate the br-GDGTs produced and prevent later modifications once available organic components inside bones are depleted. We therefore hypothesize that br-GDGTs from faunal remains may provide *in situ* paleoclimate proxies for archaeological sites on archaeologically relevant time scales.

The objectives of the present study are to: (a) demonstrate that br-GDGTs are indeed a common component in bones from archaeological sites; (b) obtain initial data on the rate of accumulation of br-GDGTs in animal bone from experimentally deposited bone at a controlled study site; (c) show that recently deposited bones from different regions display different compound distributions that reflect regional climate and environmental conditions; (d) demonstrate that br-GDGTs can be retrieved from ancient bones and matched to existing climate reconstructions, using two well-dated bone assemblages from Alaska, spanning respectively the past 30 thousand and ~1500 years.

2. Experimental

2.1. Samples

A total of 91 well-preserved animal bone samples from cultural management resource surveys and museum collections (Table 1; Figure S1) and 9 samples from a decomposition research facility (Forensic Anthropology Center at Texas State, Texas State University, San Marcos, TX) with documented artificial exposure times (Table 2) were analyzed to assess the reliability and sensitivity of the proxy across modern climate gradients. Samples represent a broad chronological range; while most date from the last 1500 years, those from the North Slope, Alaska, extend back 30,000 years. Bones were selected opportunistically, irrespective of animal types although no teeth were used (see Supplement for sample recommendations and below for discussion of bone types); no human bones were used.

Bones from recent archaeological excavation from 15 states across the U.S. roughly represent three climatic regimes, namely the northeastern and southeastern U.S. (moist regions), Arizona and New Mexico (arid region), and Alaska (cold region). All sites were open air, no samples were from caves sites without soil matrix. All bones have been stored in museum and cultural heritage collection archives. Unless otherwise noted, all bones were found disarticulated, with no indications of use and processing (burning, boiling, or cutting) or heavy post-depositional wear (gnawing or dramatic weathering).

One suite of bone samples was analyzed from sites excavated during the 1950s and early 1960s by J. Louis Giddings and Douglas Anderson of Brown University at Cape Krusenstern, on the Chukchi Sea coast, north of Kotzebue, Alaska (Giddings and Anderson, 1986). Cape Krusenstern has been occupied for the past 4200 years, since the cape

Table 1
List of animal bone samples acquired from various archaeological sites across North America. Additional information for the bone samples used in this study can be found in Table S4.

#	Region	Lab codes	Lat. (N)	Lon. (E)	C[b]	Age		MBT′	CBT	MBT′$_{5ME}$	pH		MAAT (°C)		bGDGT (ng/g)		iGDGT (ng/g)		%	
						B.P.	+/-				Avg.	+/-	Avg.	+/-	Avg.	+/-	Avg.	+/-	brGDGT	iGDGT
1	North Alaska	UAMES-02-01	69.760	−154.806	T	151	40	0.24	0.53	0.47	6.9	0.1	5.2	0.2	109.3	37.1	2.1	1.4	98.3%	1.7%
2		UAMES-07-01	69.392	−154.728	T	1093	40	0.19	0.58	0.36	6.8	0.1	3.3	0.8	90.4	21.8	7.1	4.1	93.1%	6.9%
3		UAMES-09-01	69.517	−154.883	T	2704	50	0.19	0.77	0.42	6.4	0.0	2.3	0.2	262.0	42.5	19.0	2.3	93.2%	6.8%
4		UAMES-10-01	69.401	−154.748	T	8600	50	0.20	0.28	0.30	7.4	0.3	5.5	1.0	100.0	13.1	8.5	0.8	92.2%	7.8%
5		UAMES-03-01	69.345	−154.666	T	10003	50	0.24	0.75	0.47	6.4	0.0	3.9	0.2	144.1	28.0	7.7	1.1	94.9%	5.1%
6		UAMES-06-01	69.628	−154.887	T	12473	50	0.28	0.47	0.52	7.0	0.1	7.0	0.6	9.5	2.5	3.5	0.8	72.9%	27.1%
7		UAMES-15-01	69.712	−154.839	T	14391	50	0.09	0.58	0.14	6.8	0.0	0.3	0.5	50.5	49.2	3.9	3.9	93.0%	7.0%
8		UAMES-16-01	69.515	−154.830	T	16209	50	0.13	0.66	0.19	6.6		1.0		16.7		3.4		83.0%	17.0%
9		UAMES-18-01	69.539	−154.930	T	18318	40	0.15	0.57	0.22	6.8	0.0	2.2	0.1	108.3	16.8	6.3	1.5	94.6%	5.4%
10		UAMES-19-01	69.712	−154.839	T	20362	80	0.16	0.73	0.24	6.5	0.1	1.7	0.3	355.6	67.1	19.0	5.7	95.0%	5.0%
11		UAMES-13-01	69.566	−154.927	T	21427	50	0.17	0.67	0.23	6.6	0.1	2.3	0.1	28.3	10.0	3.7	1.4	88.4%	11.6%
12		UAMES-14-01	69.593	−154.944	T	24422	80	0.11	0.77	0.22	6.4	0.0	−0.1	0.5	409.0	289.9	18.8	3.8	94.6%	5.4%
13		UAMES-05-01	70.820	−154.310	T	25844	80	0.15	0.68	0.22	6.6	0.0	1.7	0.4	99.5	6.8	18.7	0.0	84.2%	15.8%
14		UAMES-08-01	69.511	−154.836	T	26497	90	0.19	0.81	0.36	6.3	0.0	2.2	0.3	214.7	77.2	185.4	51.4	53.3%	46.7%
15		UAMES-11-01	69.058	−152.863	T	27708	90	0.16	0.78	0.28	6.4	0.3	1.5	0.5	32.8	15.3	14.0	4.0	69.2%	30.8%
16		UAMES-04-01	69.628	−154.887	T	29323	130	0.15	0.66	0.24	6.6	0.0	1.7	0.4	352.7	78.9	11.5	4.5	96.9%	3.1%
17	West Alaska	AK-09-02	67.451	−163.549	T	−10	5	0.30	1.25	0.44	5.4	0.0	2.9	1.9	3.8	2.7	0.8	0.4	80.6%	19.4%
18		AK-07-01	67.451	−163.549	M	250	50	0.28	1.14	0.52	5.7	0.0	3.1	0.2	51.8	34.7	0.6	0.6	98.9%	1.1%
19		AK-07-02	67.451	−163.549	M	250	50	0.26	1.10	0.51	5.7	0.0	2.5	0.1	356.4	33.5	8.2	1.0	97.7%	2.3%
20		AK-07-03	67.451	−163.549	M	250	50	0.25	0.95	0.53	6.0	0.0	3.3	0.2	258.6	78.8	6.5	3.2	97.6%	2.4%
21		AK-07-04	67.451	−163.549	M	250	50	0.25	0.98	0.63	6.0	0.1	3.0	0.3	225.7	44.9	6.2	1.0	97.3%	2.7%
22		AK-07-05	67.451	−163.549	M	250	50	0.29	1.22	0.49	5.5	0.0	2.9	0.1	262.1	222.4	5.0	4.2	98.0%	2.0%
23		AK-06-01	67.451	−163.549	T	250	50	0.21	0.81	0.45	6.3	0.1	2.6	0.4	275.3	23.1	6.5	3.0	97.7%	2.3%
24		AK-06-02	67.451	−163.549	T	250	50	0.22	1.25	0.58	5.4	0.0	0.7	0.3	14.6	0.3	0.9	0.1	94.2%	5.8%
25		AK-08-01	67.451	−163.549	M	900	150	0.19	0.73	0.38	6.5		2.5		69.4		1.9		97.4%	2.6%
26		AK-08-02	67.451	−163.549	M	900	150	0.28	1.03	0.50	5.9	0.0	3.5	0.1	40.9	5.0	0.7	0.2	98.2%	1.8%
27		AK-08-04	67.451	−163.549	M	900	150	0.27	0.74	0.54	6.4		4.8		17.2		1.2		93.3%	6.7%
28		AK-08-05	67.451	−163.549	M	900	150	0.21	0.52	0.49	6.9	0.0	4.4	0.7	10.8	1.6	0.9	0.2	92.5%	7.5%
29		AK-03-01	67.451	−163.549	T	900	150	0.26	0.95	0.39	6.0	0.0	3.6	0.3	556.9	179.2	6.0	1.7	98.9%	1.1%
30		AK-03-02	67.451	−163.549	T	900	150	0.25	0.91	0.42	6.1	0.0	3.4	0.7	102.6	7.1	4.0	0.8	96.3%	3.7%
31		AK-03-03	67.451	−163.549	T	900	150	0.24	0.96	0.51	6.0	0.1	2.8	0.6	44.4	33.7	4.7	2.7	89.2%	10.8%
32		AK-03-04	67.451	−163.549	T	900	150	0.29	1.03	0.56	5.9	0.0	4.1	1.0	35.8	6.2	2.9	0.2	92.5%	7.5%
33		AK-03-05	67.451	−163.549	T	900	150	0.24	0.63	0.61	6.7		4.7		19.0		0.9		95.6%	4.4%
34		AK-04-01	67.451	−163.549	M	1125	175	0.21	0.84	0.45	6.2	0.0	2.4	0.3	571.5	71.7	9.8	1.2	98.3%	1.7%
35		AK-01-02	67.451	−163.549	T	1125	175	0.18	0.97	0.36	6.0	0.0	1.0	0.2	37.0	0.7	4.2	0.1	89.8%	10.2%
36		AK-01-03	67.451	−163.549	T	1125	175	0.16	0.85	0.51	6.2	0.0	0.9	0.5	29.7	2.0	5.8	0.1	83.6%	16.4%
37		AK-01-04	67.451	−163.549	T	1125	175	0.22	0.66	0.36	6.6	0.0	4.0	0.1	153.7	13.2	9.7	0.6	94.0%	6.0%
38		AK-01-05	67.451	−163.549	T	1125	175	0.24	1.00	0.45	5.9	0.1	2.7	0.4	400.2	72.7	8.0	0.9	98.0%	2.0%
39		AK-01-06	67.451	−163.549	T	1125	175	0.21	1.06	0.47	5.8	0.5	1.3	1.7	83.8	16.0	10.5	4.2	89.1%	10.9%
40		AK-01-07	67.451	−163.549	T	1125	175	0.20	1.11	0.45	5.7		0.8		102.7		5.6		94.8%	5.2%
41		AK-01-08	67.451	−163.549	T	1125	175	0.18	0.83	0.35	6.3	0.0	1.7	0.2	253.1	307.5	1.3	1.5	99.4%	0.6%
42		AK-01-09	67.451	−163.549	T	1125	175	0.17	0.86	0.33	6.2		1.1		175.8		10.4		94.4%	5.6%
43		AK-01-10	67.451	−163.549	T	1125	175	0.22	1.09	0.36	5.8	0.1	1.5	0.7	99.2	13.0	10.8	1.6	90.2%	9.8%
44		AK-01-11	67.451	−163.549	T	1125	175	0.24	0.99	0.43	6.0	0.0	2.6	0.3	132.2	19.1	11.0	1.8	92.3%	7.7%
45		AK-05-01-A[a]	67.451	−163.549	M	1350	50	0.33	1.32	0.47	5.3	0.6	3.7	1.8	276.5	233.7	9.4	3.3	95.7%	4.3%
46		AK-05-01-B[a]	67.451	−163.549	M	1350	50	0.27	0.73	0.41	6.5	0.7	5.0	2.1	226.0	154.8	35.7	34.6	89.6%	10.4%
47		AK-05-02-A[a]	67.451	−163.549	M	1350	50	0.29	1.01	0.43	5.9		4.2		69.7		3.3		95.5%	4.5%

(*continued on next page*)

Table 1 (*continued*)

#	Region	Lab codes	Lat. (N)	Lon. (E)	C[b]	Age		MBT′	CBT	MBT′$_{5ME}$	pH		MAAT (°C)		bGDGT (ng/g)		iGDGT (ng/g)		%	
						B.P.	+/-				Avg.	+/-	Avg.	+/-	Avg.	+/-	Avg.	+/-	brGDGT	iGDGT
48		AK-05-02-B[a]	67.451	−163.549	M	1350	50	0.28	0.89	0.47	6.1	0.0	4.4	0.8	25.0	8.0	1.6	0.5	94.0%	6.0%
49		AK-05-03	67.451	−163.549	M	1350	50	0.27	0.92	0.44	6.1		4.0		188.8		5.5		97.2%	2.8%
50		AK-05-04	67.451	−163.549	M	1350	50	0.30	1.05	0.45	5.8	0.0	4.1	0.3	1395.1	2.7	30.8	9.1	97.8%	2.2%
51		AK-05-05	67.451	−163.549	M	1350	50	0.25	1.56	0.39	4.8	0.1	−0.4	0.2	388.3	26.5	1.3	0.2	99.7%	0.3%
52		AK-05-06	67.451	−163.549	M	1350	50	0.34	1.52	0.49	4.9		2.7		156.0		4.3		97.3%	2.7%
53		AK-02-01-A[a]	67.451	−163.549	T	1350	50	0.16	0.80	0.40	6.3		1.3		186.0		17.6		91.4%	8.6%
54		AK-02-01-B[a]	67.451	−163.549	T	1350	50	0.17	0.98	0.40	6.0	0.2	0.5	0.8	196.1	65.0	14.9	4.4	92.9%	7.1%
55		AK-02-02-A[a]	67.451	−163.549	T	1350	50	0.32	0.92	0.54	6.1		5.6		39.6		3.2		92.5%	7.5%
56		AK-02-02-B[a]	67.451	−163.549	T	1350	50	0.17	0.70	0.39	6.5	0.3	2.0	1.0	109.4	105.4	7.9	8.0	93.5%	6.5%
57		AK-02-03	67.451	−163.549	T	1350	50	0.25	0.87	0.44	6.2	0.1	3.8	0.9	507.2	124.7	23.3	8.2	95.7%	4.3%
58		AK-02-05	67.451	−163.549	T	1350	50	0.18	0.76	0.54	6.4	0.0	2.2	0.1	82.0	43.2	17.5	8.0	82.1%	17.9%
59		AK-02-09	67.451	−163.549	T	1350	50	0.18	0.81	0.45	6.3	0.1	1.7	0.0	0.9	0.4	0.2	0.1	85.1%	14.9%
60		AK-05-07	67.451	−163.549	T	1350	50	0.25	1.01	0.49	5.9	0.0	3.0	0.1	44.5	15.5	4.1	1.2	91.6%	8.4%
61	East Coast, U.S.	PAL-01-01	42.296	−71.713	T			0.42	0.26	0.76	7.4	0.0	12.2	0.3	227.4	57.5	3.0	1.5	98.7%	1.3%
62		PAL-02-01-A[a]	42.588	−72.601	T			0.39	0.34	0.55	7.2		10.9		1106.1		515.9		68.2%	31.8%
63		PAL-02-01-B[a]	42.588	−72.601	T			0.41	0.45	0.70	7.0		11.0		210.4		48.2		81.4%	18.6%
64		PAL-03-01	42.279	−71.150	T			0.61	0.53	0.77	6.8	0.0	16.6	0.0	192.0	57.7	65.8	18.8	74.4%	25.6%
65		PAL-04-01	42.491	−71.276	T			0.29	0.83	0.46	6.3	0.0	5.1	0.2	507.9	75.6	255.2	60.3	66.8%	33.2%
66		PAL-05-01	42.051	−72.772	T			0.42	0.63	0.91	6.6		10.2		142.2		1443.0		9.0%	91.0%
67		PAL-06-01	41.344	−70.815	T			0.44	0.58	0.65	6.8	0.0	11.2	0.0	70.2	14.5	7.7	1.8	90.2%	9.8%
68		PAL-07-01	41.945	−71.286	T			0.50	0.71	0.79	6.5	0.0	12.2	0.4	56.0	12.2	26.6	5.8	67.8%	32.2%
69		PAL-08-01-A[a]	41.266	−70.068	T			0.47	0.68	0.71	6.6		11.5		1187.8		134.7		89.8%	10.2%
70		PAL-08-01-B[a]	41.266	−70.068	T			0.49	0.57	0.86	6.8		12.7		310.1		25.6		92.4%	7.6%
71		PAL-09-01	45.189	−67.279	T			0.37	0.47	0.86	7.0	0.0	9.5	0.2	29.8	9.8	63.9	29.5	32.7%	67.3%
72		PAL-11-01	40.622	−74.245	T			0.44	0.30	0.54	7.3		12.7		1147.2		2943.0		28.0%	72.0%
73		PAL-12-01	42.598	−73.822	T			0.30	0.12	0.67	7.7		9.5		115.7		294.9		28.2%	71.8%
74		PAL-13-01	39.831	−77.231	T			0.34	0.05	0.59	7.8	0.0	11.2	0.0	115.0	34.4	319.8	86.9	26.4%	73.6%
75		PAL-14-01	41.831	−71.541	T			0.44	0.40	0.79	7.1	0.0	12.1	0.4	137.1	48.1	423.6	212.7	25.3%	74.7%
76		PAL-15-01	41.781	−71.437	T			0.46	0.42	0.78	7.1		12.8		142.7		97.5		59.4%	40.6%
77		PAL-16-01	43.390	−72.471	T			0.29	0.11	0.56	7.7		9.1		161.3		43.2		78.9%	21.1%
78		PAL-17-01	41.982	−72.651	T			0.57	0.21	0.79	7.5	0.0	17.2	0.3	247.9	65.6	138.5	34.7	64.0%	36.0%
79		TRC-01-01	35.182	−83.382	T	50	25	0.55	0.47	0.86	7.0	0.0	15.3	0.2	130.2	34.5	168.6	52.5	43.9%	56.1%
80		TRC-01-02	35.182	−83.382	T	50	25	0.57	0.56	0.90	6.8	0.0	15.2	0.3	181.3	49.7	190.6	76.5	49.6%	50.4%
81		TRC-01-03	35.182	−83.382	T	50	25	0.58	0.20	0.79	7.5	0.0	17.6	0.2	357.6	65.3	293.8	83.0	55.4%	44.6%
82		TRC-02-01	32.426	−80.591	T	150	25	0.51	0.10	0.80	7.7	0.0	15.9	0.2	82.0	12.6	141.0	24.1	36.8%	63.2%
83		TRC-02-02	32.426	−80.591	T	150	25	0.45	0.24	0.92	7.4	0.1	13.4	0.1	36.5	3.3	18.8	2.1	66.0%	34.0%
84		TRC-02-03	32.426	−80.591	T	150	25	0.55	0.19	0.93	7.5	0.1	16.8	0.2	41.9	4.7	18.3	0.1	69.6%	30.4%
85	Southwest, U.S.	TRW-03-01	35.777	−103.957	T	50	10	0.15	1.26	0.90	5.4		−1.6		84.7		56.1		60.1%	39.9%
86		TRW-03-02	35.777	−103.957	T	50	10	0.13	1.46	0.93	5.0		−3.5		54.4		44.2		55.1%	44.9%
87		TRW-02-01	32.722	−109.105	T	600	25	0.12	0.98	0.75	6.0	0.3	−1.0	0.7	72.4	63.5	127.9	82.2	31.6%	68.4%
88		TRW-04-01	32.436	−111.222	T	900	25	0.45	1.18	1.00	5.6		8.0		221.5		111.6		66.5%	33.5%
89		TRW-04-02	32.436	−111.222	T	900	25	0.34	1.13	0.99	5.7		5.0		74.6		52.5		58.7%	41.3%
90		TRW-01-01	32.404	−111.049	T	1400	50	0.35	1.36	0.94	5.2		4.0		108.4		165.3		39.6%	60.4%
91		TRW-01-02	32.404	−111.049	T	1400	50	0.39	1.25	0.93	5.4	0.4	5.7	0.2	101.0	79.3	48.8	4.1	62.4%	37.6%

[a] Selected long bones were sawed into two separate samples prior to ASE extraction: ID-XX-XX-A (spongy bone) and ID-XX-XX-B (compact bone).

[b] Category of samples: T = terrestrial animal bones; M = Marine animal bones.

Table 2
List of bone (pig) and soil samples acquired from the Forensic Anthropology Center at Texas State, Texas State University, San Marcos, TX.

#	Sample	Lat. (N)	Lon. (E)	Type	Age			MBT′	CBT	MBT'_{5ME}	pH		MAAT (°C)		bGDGT (ng/g)		iGDGT (ng/g)		%	
					Start	Stop	Years				Avg.	+/-	Avg.	+/-	Avg.	+/-	Avg.	+/-	brGDGT	iGDGT
1	BODY-01	29.940	−98.008	Bone	2015/11	2016/07	0.75		N/A											
2	BODY-02	29.940	−98.008	Bone	2012/05	2016/07	4.17	0.56	1.32	0.82	5.3	0.1	9.6	0.0	22.5	12.9	8.5	5.0	72.7%	27.3%
3	BODY-03	29.940	−98.008	Bone	2012/03	2016/07	4.33	0.32	1.04	0.77	6.0		0.0		60.0		27.5		68.6%	31.4%
4	BODY-04-A	29.940	−98.008	Bone	2007/08	2016/07	8.92	0.47	1.35	0.83	5.2	0.0	4.7	0.3	61.1	38.4	147.8	72.6	28.4%	71.6%
5	BODY-04-B	29.940	−98.008	Bone	2007/08	2016/07	8.92	0.53	1.22	0.86	5.5		8.9		122.6		90.8		57.5%	42.5%
6	BODY-04-C	29.940	−98.008	Bone	2007/08	2016/07	8.92	0.45	1.40	0.86	5.1	0.2	3.4	0.9	17.6	8.9	15.3	5.8	52.1%	47.9%
7	BODY-01	29.940	−98.008	Soil	2015/11	2016/07	0.75	0.66	0.81	0.81	7.2	0.9	12.4	8.2	547.3	322.7	53.5	54.5	92.5%	7.5%
8	BODY-03	29.940	−98.008	Soil	2012/03	2016/07	4.33	0.47	0.83	0.70	6.6		9.5		555.7		72.4		88.5%	11.5%
9	BODY-04	29.940	−98.008	Soil	2007/08	2016/07	8.92	0.60	1.12	0.81	5.8		13.6		528.2		23.3		95.8%	4.2%

began to form in a context of regionally stabilizing sea levels (Anderson et al., 2014; Anderson and Freeburg, 2014; Mason and Ludwig, 1990). The analyzed bone samples come from domestic deposits that represent five occupation phases at Cape Krusenstern spanning the past 1450 years: Ipiutak (House 40, c. 550-750 AD), Birnirk (House 32, c. 700-950 AD), Western Thule (House 4, c. 950-1250 AD), Old Kotzebue (House 35, c. 1650-1750 AD), and Modern (1955-1965 AD).

Samples from the University of Alaska Museum in Fairbanks (UAMES) are from an archival collection of megafauna bones collected from point bars and eroding bluffs along the upper 80 km of the Ikpikpuk and Titaluk Rivers and their tributaries (Table 1; Figure S1) (Mann et al., 2013). These bones have been collected almost annually since 1998 on foot and in canoes, with a varying extent of systematic coverage. It is important to note that unlike the other samples, these were not recovered with formal archaeological methods, and while documented in terms of position are largely without context. Furthermore, some samples, including UAMES-11 were collected from other North Slope alluvial river valleys. These bones were useful in that they were in good condition (bone weathering stages 0, 1, and 2 of Behrensmeyer, 1978) and had been used in a prior radiocarbon dating and stable isotope study on Ice-Age Arctic megafauna (Mann et al., 2013). These bones were exceptionally preserved as they were in frozen and/or anaerobic sediment in the floodplains of these rivers.

Public Archaeology Laboratory (PAL) graciously provided samples from their animal bone assemblages from post-contact (non-Native American) sites from the 17th-20th centuries from both anthropic and alluvial fills in Weathersfield (Vermont), Suffield (Connecticut), Calais (Maine), Gettysburg (Pennsylvania), Linden (New Jersey), Bethlehem (New York), Cranston and Johnston (Rhode Island), and Shrewsbury, Greenfield, Nantucket, West Roxbury, Attleboro, Aquinnah, Bedford, and Southwick (Massachusetts). Tierra Right of Way Solutions provided samples from Marana and Torolita (New Mexico) and Duncan (Arizona) dating from the 6th, 11th, 14th and 20th centuries CE from anthropic features fills; TRC Solutions contributed samples from Franklin (North Carolina) and Dataw Island (South Carolina).

2.2. Sample preparation

The bones were thoroughly rinsed with deionized water. The periosteal and endosteal surfaces were scraped away as necessary to avoid contamination. The samples were pulverized using a mortar and pestle, sieved at 425 μm openings, homogenized, and extracted with dichloromethane/methanol (DCM:MeOH) (9:1, v/v) using an accelerated solvent extractor (Dionex ASE 200) at 120 °C and 1200 psi. The total lipid extract (TLE) was evaporated to dryness under nitrogen and separated into apolar and polar fractions using an alumina (Al_2O_3) column by liquid chromatography using Hexane:DCM (1:1, v/v) and DCM:MeOH (1:1, v/v) respectively. The polar fractions containing brGDGTs were dissolved in 500 μL of hexane/isopropanol (99:1, v/v) and combined with 5 μL of a C_{46} synthetic GDGT internal standard (0.0126 mg/mL stock solution) for quantification on HPLC-MS.

2.3. HPLC/MS

The HPLC system (Agilent 1200 series) consisted of a solvent degasser (G1379B), binary pump (G1312A), thermostatted column compartment (G1316A), autosampler (1329A), and two Waters BEH HILIC columns (1.7 μm, 150 mm × 2.1 mm i.d.) arranged in series. The HPLC was coupled to a quadrupole mass spectrometer (Agilent 6130 series) equipped with an atmospheric pressure chemical ionization (APCI) probe. The samples were separated using a method adapted from Hopmans et al. (2016) with a mobile phase gradient of hexane (solvent A) and hexane/isopropanol (9:1, v/v) (solvent B) with a flow rate of 0.2 mL/min and column temperature of 30 °C. They were treated in an initial mobile phase (solvent A: 82%; solvent B: 18%) that was held for 25 min, followed by a second gradient (solvent A: 65%; solvent B: 35%)

for 25 min, and a final gradient (solvent A: 0%, solvent B:100%) for 30 min. The column was re-equilibrated to the initial mobile phase (solvent A: 82%, solvent B: 18%) for 20 min following completion of the run.

The samples were analyzed for both br-GDGTs and isoprenoidal GDGTs (i-GDGTs here after) using selected ion monitoring (SIM) of the following ions: 744 (C_{46} GDGT standard), 1018, 1020, 1022, 1032, 1034, 1036, 1046, 1048, 1050, 1292, 1296, 1298, 1300, 1302 (Tables S1 and 2). Typical injection volumes ranged from 10 to 25 µL. We currently do not have a calibration for br-GDGTs in bones to convert our data to temperature, pH, and precipitation values, therefore existing soil calibrations were used in this study (De Jonge et al., 2014; Peterse et al., 2012; Yang et al., 2014).

3. Results and discussion

3.1. GDGTs are present in all bones from archaeological sites

We examined 91 bone samples from archaeological sites from three macro-regions across North America (Table 1). While the precise ages of these bones are not known (except for radiocarbon dated bone samples from northern and western Alaska), they mostly date from historic periods and thus reflect climate conditions within the recent past (ca. 1800–1950). Variable amounts of br-GDGTs and i-GDGTs are found in these samples. Bone samples originating from the East Coast contain, on average, ca. 160 ng/g of i-GDGTs and br-GDGTs, respectively (Fig. 1). Samples from Alaska contain a slightly lower amount of br-GDGTs (average 120 ng/g) but have a wide range of up to 600 ng/g. Br-GDGTs are least represented in samples from the American Southwest (~70 ng/g). In contrast, i-GDGTs have the lowest quantity in the Alaskan samples but are relatively abundant in East Coast and southwestern samples. The southwestern samples contain the highest relative percentages of i-GDGTs, whereas the Alaskan samples are dominated by br-GDGTs (> 80% of total GDGTs), with the East Coast samples are between the southwestern and Alaskan ones. It is important to note that the relative differences in i- and br-GDGTs in bone samples are like those observed in soils. Many studies have shown that soils in arid regions tend to contain greater proportions of i-GDGTs (Dirghangi et al., 2013; Xie et al., 2012; Yang et al., 2014), whereas soils in Arctic regions are dominated by br-GDGTs (Weijers et al., 2007a; Shanahan et al., 2013).

A closer look at the distributions of individual br- and i-GDGTs reveals additional regional characteristics (Figure S2; Table S1). While most common i-GDGTs found among all samples were the uncyclized GDGT 0 (1302 *m/z*), cyclohexane-containing GDGT crenarchaeol and the crenarchaeol regio-isomer (1292 *m/z*), the relative amounts of other i-GDGTs, including GDGT I (1300 *m/z*/), GDGT II (1298 *m/z*/), and GDGT III (1296 *m/z*/), vary significantly by region. The bulk of the i-GDGTs in the northern Alaskan samples is made up by crenarchaeol GDGTs (~90–100% of the isoprenoid GDGT distribution), whereas samples from the western Alaska coastal region contain significant amounts of GDGT 0, accounting for up to ~25% of the total isoprenoid distribution. Samples from the U.S. East Coast typically contain lower amounts of the crenarchaeol GDGT and GDGT 0 but higher quantities of GDGT I, II and III relative to the Alaskan samples. Samples from the southwestern U.S. display a distinct i-GDGT signature, with crenarchaeol accounting for approximately 40–60% of the isoprenoid content. As noted above, the signatures of i-GDGTs in these bone samples are in general agreement with the results from soil samples from Arctic, arid, and temperate regions (Dirghangi et al., 2013; Weijers et al., 2007a; Yang et al., 2014). However, the relatively higher concentration of crenarchaeol GDGTs in the northern Alaskan fluvial samples is more consistent with the relative high concentration of this compound in marine and lake sediments (Tierney et al., 2012). Crenarchaeol is relatively uncommon in soils (e.g., Weijers et al., 2007a) hence its high concentration in bones may originate from the unique micro-environmental conditions inside the bones. These distinct i-GDGT profiles further support that these tetra-ether lipids, including br-GDGTs, are produced *in situ* in bones rather than migrated from soils.

The br-GDGT peaks also show clear differences in relative abundance across each region. As anticipated, temperature is a key factor affecting br-GDGT distributions from the Alaskan and East Coast samples. Higher latitude samples tend to contain greater amounts of methyl substitutions at the 5′ or 6′ positions of the br-GDGT backbone (i.e. more GDGT IIIa, 1050 *m/z*), whereas samples from lower latitude, and thus warmer, regions contained less methylation (i.e. more GDGT Ia, 1022 *m/z*). While the Alaskan samples do show lower inferred temperatures than the East Coast samples, MBT'/CBT inferred annual mean temperatures from Alaskan samples are much higher than modern values in Alaska (Figs. 1 and 2A). Similar cold bias is also observed when we apply MBT'_{5ME} calibration (Naafs et al., 2017) that excludes 6-methyl br-GDGTs. We attribute this anomaly to biased seasonal activity of the bacteria in Alaska, where the winters are too cold for the br-GDGT-producing bacteria to grow. Since br-GDGTs are mainly produced during the warm summer, they reflect the higher average season temperature. A similar seasonal bias has been proposed to explain abnormally high br-GDGT inferred temperatures from the high altitude Tibetan plateau (Dang et al., 2016; De Jonge et al., 2014; Peterse et al., 2012). Samples from the southwestern U.S. conversely display a major cold bias (Figs. 1 and 2A), which has been well documented in many soils from arid regions when MBT'/CBT calibration is used (Dang et al., 2016; De Jonge et al., 2014; Dirghangi et al., 2013; Peterse et al., 2012). This effect is thought to be related to depleted soil moisture and/or low precipitation. The br-GDGT-inferred temperatures from soils in arid southern Utah are for instance below 0 °C, whereas the actual mean annual temperatures fall in the range of 10–15 °C (Dirghangi et al., 2013). Interestingly, however, when we apply the more recent calibration based on MBT'_{5ME} (Naafs et al., 2017), the br-GDGT-inferred temperatures from southwest bone samples are generally consistent with environmental temperatures (Fig. 2B).

Soils from the East Coast of the United States that show generally increasing MBT′ inferred temperature and latitude. These coastal regions have high precipitation and have previously been shown to reflect temperatures well based on br-GDGT distributions (Dirghangi et al., 2013). There remain, nevertheless, considerable discrepancies between the MBT'/CBT-inferred temperatures and latitude, partly because of chronological differences in our bone samples.

The pH values inferred from the CBT index do not appear to correlate with corresponding soil pH values (Fig. 1B). Soils in the arid southwestern regions generally have higher pH values than the moist and productive eastern coastal regions, where soils tend to be acidic. We observe the opposite trend, with East Coast samples showing higher pH values in bone samples. We suggest that this may be due to the inorganic part of bones that is composed of hydroxyapatite carbonate ($Ca_5(PO_4)_3(OH)$), which dissolves over time to form a phosphate-rich buffering solution, altering the CBT-inferred pH values. Therefore, we suggest that br-GDGTs in bones may attenuate the pH signal of soil conditions (if they serve as a total buffer, we would expect uniform values of pH).

Principal component analysis (PCA) provided a more quantitative look at differences among the three geographic regions (Fig. 3). PCA was performed using the relative abundances of the br-GDGTs Ia, Ib, Ic, IIa IIb, IIc, and IIIa, including both 5′ and 6′ isomers for br-GDGTs II and III. The first principal component accounted for approximately 37.2% of the variance, with the second principal component accounting for 21.5% (explaining a cumulative variance of 58.7%). The abundance of these three br-GDGTs provided a simple and distinctive regional fingerprint for sample origin identification. Results from PCA basically indicate that br-GDGTs from our three study regions (Alaska, Southwest, and East Coast) show distinctive differences that likely reflect regional climatic and environmental differences.

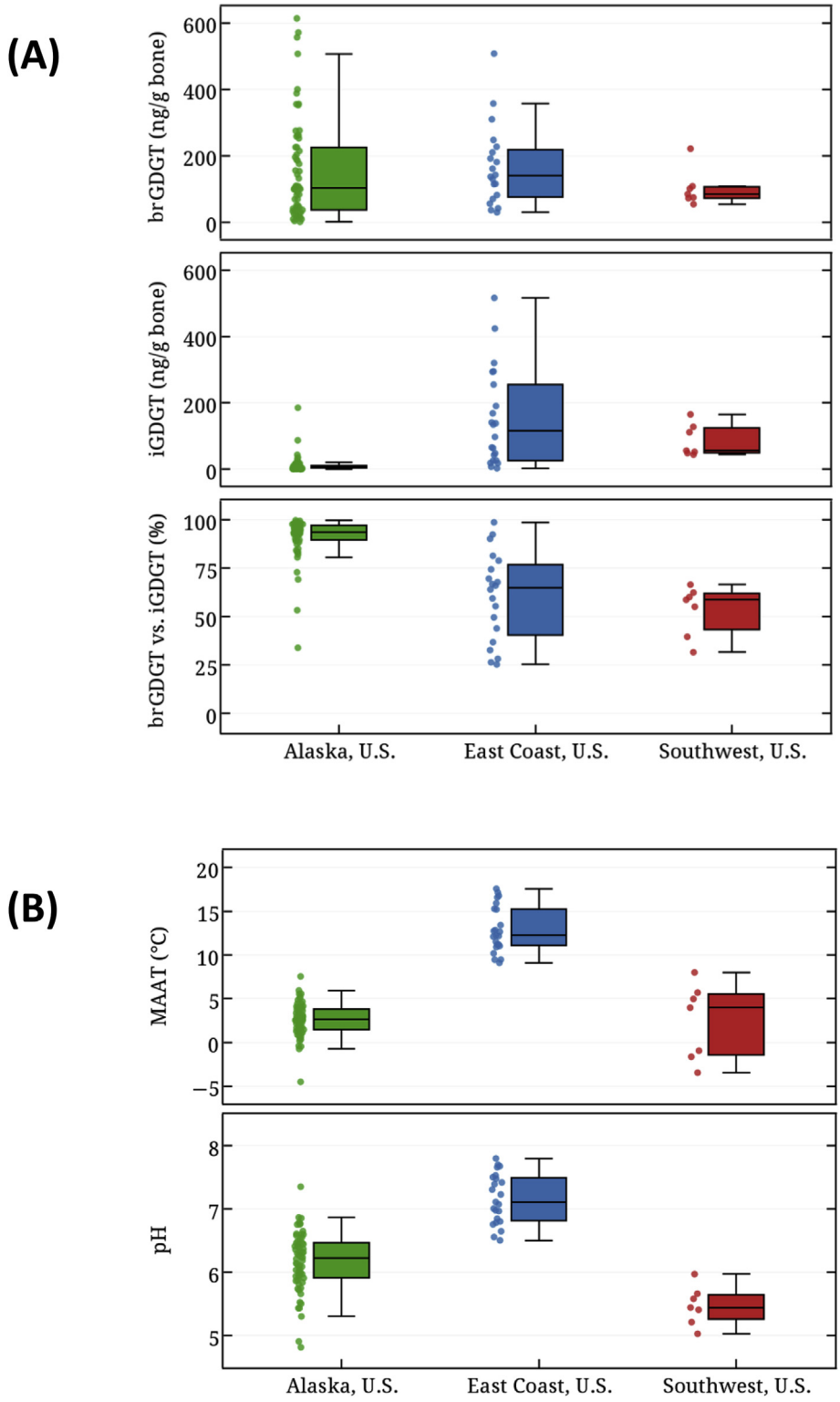

Fig. 1. (A) Abundance of br- and i-GDGTs (ng/g of bone) from bone samples analyzed in this study. Samples are from three regions in the United States: a) Alaska; b) East Coast; c) Southwest. **(B)** Box plots of the MBT′ and CBT inferred mean annual mean temperature (MAAT, ˚C) and pH of all bone samples analyzed in this study.

3.2. Evidence for in situ production of br-GDGTs in bones

In addition to our observed abnormally high abundance of crenarchaeol in bones discussed above, we studied bone samples from the decomposition research facility at the Forensic Anthropology Center (FAC) of Texas State University in San Marcos, Texas (Table 2 & Table S2), in order to further investigate if br-GDGTs are indeed produced *in-situ* by bacteria inside bones. We obtained pig bone samples that had been left in the field for 1, 4 and 9 years, respectively. The advantages of using the FAC samples are that we know how long the bodies of these pigs had been decomposing in monitored climatic conditions. We also obtained soils from the same disposal site for comparison.

No br-GDGTs were detected in fresh bones. As the time of decomposition increased, we found a gradual increase in br-GDGT abundance,

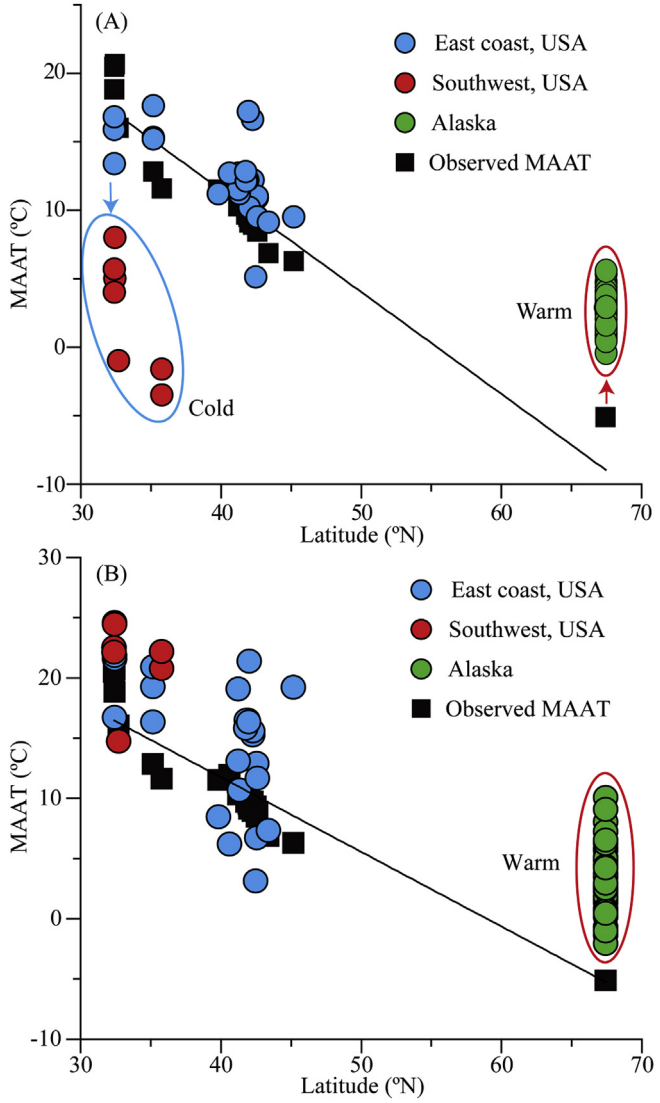

Fig. 2. (A) The relationships between MBT'/CBT (Peterse et al., 2012; MAT = 0.81 + 31.0 × MBT'-5.67 × CBT; R^2 = 0.58, n = 219, RMSE = 5.5 °C) inferred temperatures and latitudes in bone samples in Table 1; and (B) The relationships between MBT'_{5ME} (Naafs et al., 2017; $MAAT_{soil}$ = 40.01 × MBT'_{5ME}-15.25; R^2 = 0.66, n = 222, RMSE = 4.8 °C) inferred temperatures and latitudes in bone samples in Table 1. Black squares represent 1960–2000 average temperatures for the same archaeological sites where bone samples are recovered, based on online WorldClim database (http://worldclim.org).

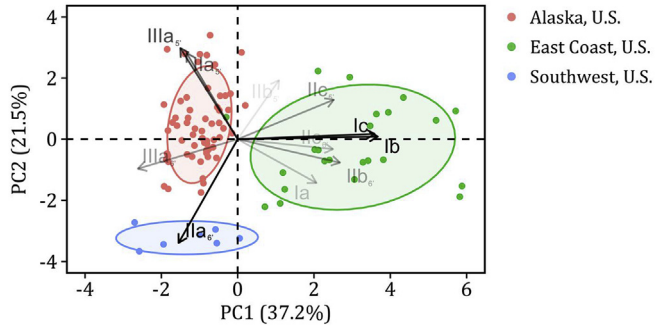

Fig. 3. Principal component analysis (PCA) of br-GDGTs from the collection of bone samples used in this study. PCA based on relative abundances of 11 branched-GDGTs: Ia. Ib, Ic, IIa, IIa', IIb, IIb', IIc, IIc', IIIa, and IIIa'.

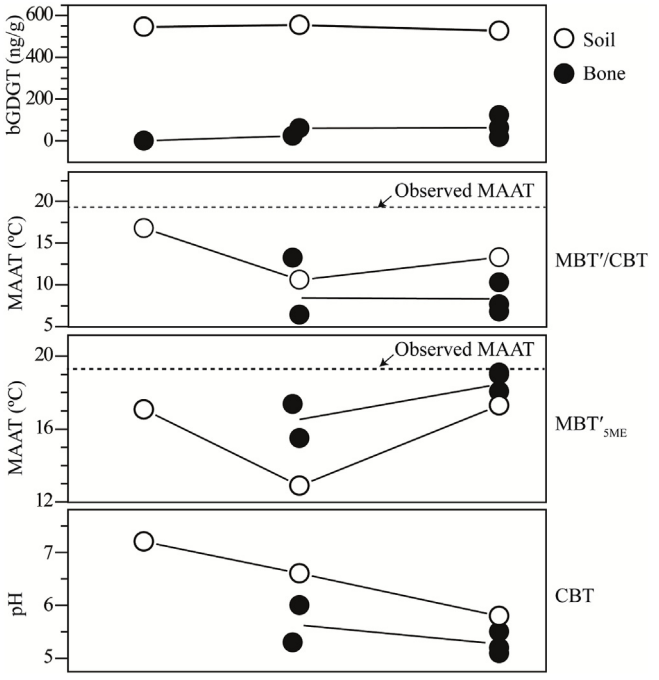

Fig. 4. *In situ* production of br-GDGTs in artificially decomposed animal bones, measured after 1, 4, and 9 years of field decomposition in soils. Results computed using calibrations of MBT'/CBT (Peterse et al., 2012; MAAT = 0.81 + 31.0 × MBT'-5.67 × CBT; R^2 = 0.58, n = 219, RMSE = 5.5 °C) and MBT'_{5ME} (Naafs et al., 2017; $MAAT_{soil}$ = 40.01 × MBT'_{5ME} - 15.25; R^2 = 0.66, n = 222, RMSE = 4.8 °C) are plotted for comparison. CBT-inferred pH values are also plotted.

suggesting continuous growth of the bacteria that produce these compounds (Fig. 4). The concentrations of br-GDGTs in bones were nevertheless significantly lower than those in surrounding soils, even after nine years of natural decomposition. These data support our hypothesis that br-GDGTs inside the bones are indeed produced *in situ*, that is within the bones. The FAC facility is in a relatively warm and moist region with an annual mean rainfall of 914 mm, which is concentrated in spring and fall; the annual mean temperature is 20 °C. This climate is well suited to the growth of br-GDGT-producing bacteria, and soils in this region would have produced br-GDGTs throughout the year, if fresh organic matter is available. Our data show that br-GDGTs may require more than 9 years before a reliable and stable signal is obtained, consistent with previous study by Weijers et al. (2010) suggesting a turnover rate of 18 years in soils.

However, temperatures inferred from bone br-GDGTs using the MBT'/CBT index (Peterse et al., 2012) are 2–5° lower, whereas those inferred from MBT'_{5ME} index (Naafs et al., 2017) are 2–5° higher, than those inferred from surrounding soils (note that the concentration of br-GDGTs in the one-year old bone sample was too low for index calculations). All br-GDGT-inferred temperatures are lower than observed mean annual temperature (Fig. 4). There are a few possible reasons for this discrepancy. First, the three soil samples also show more than 5°C differences in br-GDGT inferred temperatures, and this wide range of variation indicates significant heterogeneity of local soils and perhaps of different microenvironments at the same site. Secondly, it is possible that the microbial communities in the bones that produce br-GDGTs differ significantly from those in the surrounding soils. Bones contain much higher concentrations of nutrients (phosphorus and nitrogen) and organic materials but may contain less moisture than the surrounding soils, which could significantly affect the microbial communities. As discussed earlier, a reduction in available moisture could lead to significantly lower temperatures as inferred from MBT'/CBT index. On the other hand, the MBT'_{5ME} inferred temperatures from the 9-year old

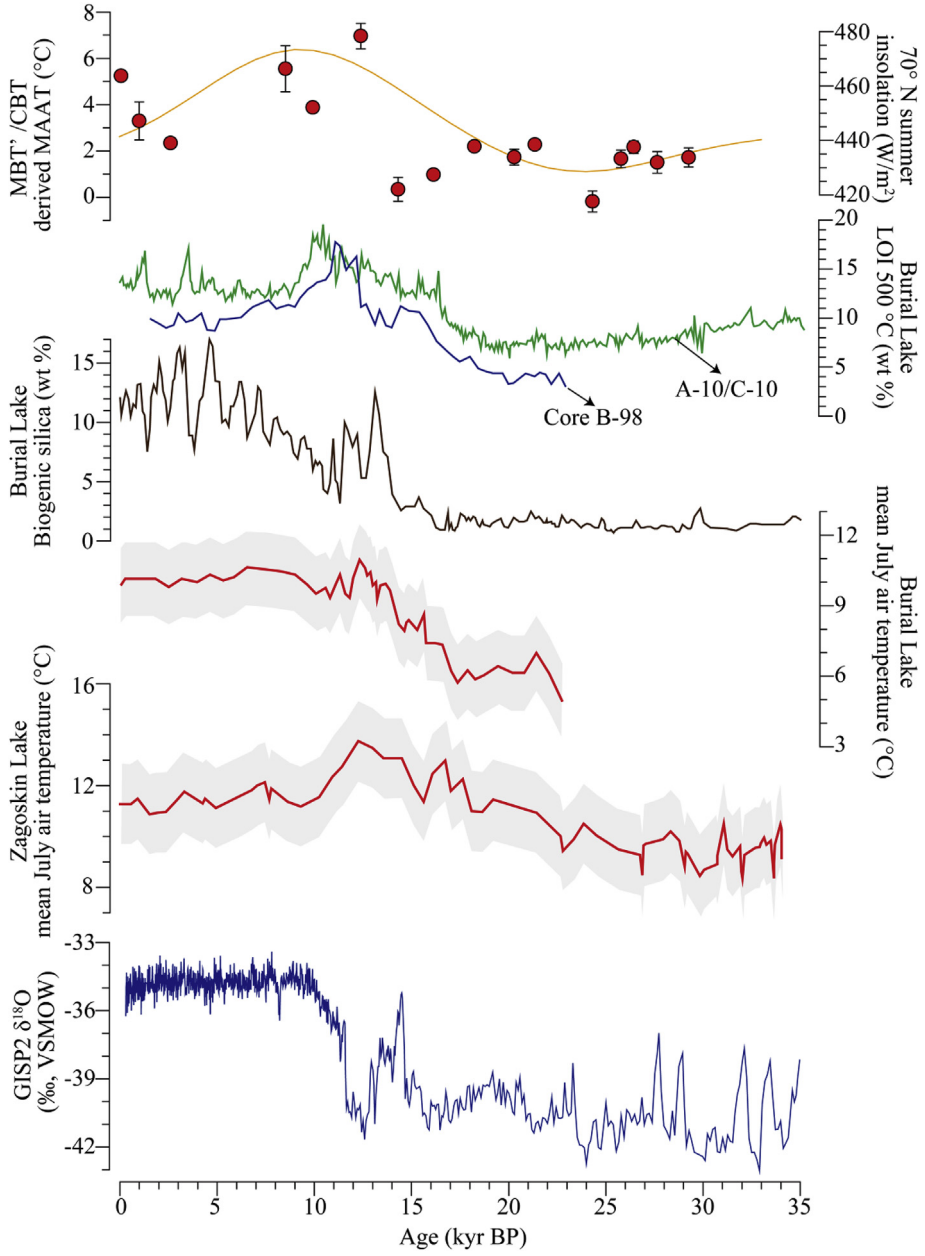

Fig. 5. Reconstructed MAAT of North Slope, Alaska using radiocarbon dated bone samples based on contents of branched-GDGTs, and comparison with published regional temperature changes and limnology data. MBT'/CBT calibration is used here (Peterse et al., 2012).

bone samples are approaching the observed mean annual temperature (Fig. 4). A more robust temperature calibration for bone br-GDGTs would require analysis of modern (sufficiently weathered so that br-GDGT distributions reach a steady state with surrounding environment) bone samples from a wider range of climate conditions (Weijers et al., 2007b), and probably take into consideration 5- and 6-methyl br-GDGTs separately (Naafs et al., 2017).

3.3. Bones from chronologically controlled sequences record past climate variations

We analyzed two sets of well-dated ancient bone samples from Alaska to demonstrate that br-GDGTs inside the bones indeed record past temperature and that such temperature signals are preserved. br-GDGTs have been preserved in marine and lake sediments and loess soils for tens of thousands to millions of years (Gao et al., 2012; Weijers et al., 2007a), suggesting these compounds are diagenetically highly stable in natural environmental settings. It is unlikely that diagenetic alternation in bones would be dramatically faster than in the natural soils and sediments in which they are buried. While comparisons of other chemical proxies, such as stable isotopes, in shells and bones show that diagenetic processes caused by leaching and recrystallization constrain results, our analyses focus on biomarkers deposited in the bone after deposition and not on compounds deposited in the animal during its lifetime.

The first set of bone samples is from the collection of the University of Alaska's Museum of the North (Table 1). These bones were collected from various sites in northern Alaska and have radiocarbon dates that span the past 30,000 years. We analyzed br-GDGTs in these bone samples and computed inferred temperatures using various published calibrations for MBT'/CBT (De Jonge et al., 2014; Peterse et al., 2012) (Fig. 5), and other indices, including MBT_{5Me} (De Jonge et al., 2014), and Index 1 (De Jonge et al., 2014) (Table S3; Figures S3). All three indices show similar trends, but the amplitude of temperature change

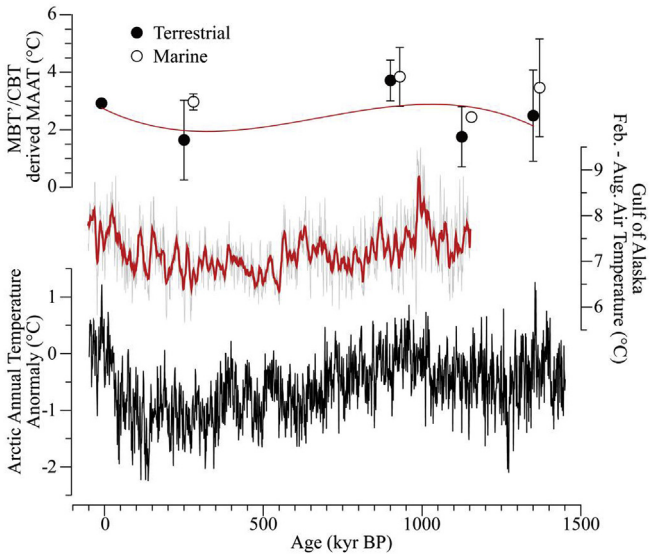

Fig. 6. Comparison of reconstructed MAAT of Cape Krusenstern, Alaska using bone derived branched-GDGTs with published temperature reconstructions. MBT'/CBT calibration is used here (Peterse et al., 2012).

from the last glacial maximum to the early Holocene is likely too large when calibrated with MBT_{5Me}, because the chironomid-inferred temperature reconstructed at the Burial Lake site in the foothills of the Brooks Range suggests approximately 5 degrees of change (Kurek et al., 2009). Both MBT'/CBT and Index 1 inferred temperatures show similar amplitudes of temperature change from the last glacial maximum to the Early Holocene (~5 °C), but the absolute temperatures inferred from MBT'/CBT are a few degrees higher. These temperatures are significantly higher than the annual mean temperatures for northern Alaska, consistent with our br-GDGT-inferred temperatures being biased towards the summer season in very cold regions.

Because these bone samples had a relatively low chronological resolution, it is difficult to hone in on the exact timing of the deglacial temperature rise in this suite of samples. Both our bone br-GDGT-inferred temperatures and the chironomid-inferred temperatures from Burial Lake show, however, a relatively early start of the temperature rise compared to the isotope records from the Greenland ice cores (Fig. 5). The timing of our deglacial temperature rise also matches well with the abrupt productivity increase of diatoms in Burial Lake, as recorded by the biogenic silica (Finkenbinder et al., 2015).

The chironomid-inferred temperatures from Zagoskin Lake in western Alaska, by contrast, show a much earlier date for the deglacial temperature rise than what either the Burial Lake chironomids or our bone samples suggest. Assuming that all proxy records are correct, it is likely that there is a west-to-east time-transgression in deglacial warming, which would correspond to a west-to-east progression during melting of the Laurentide Ice Sheet (Kaufman et al., 2004). The peak temperatures as inferred from br-GDGTs, Burial Lake and Zagoskin Lake chironomids are nevertheless consistent in identifying the period around 12–14 kyr as the warmest time during the Bølling-Allerød events in the Alaska region (Kurek et al., 2009). For the Holocene, bone-inferred temperatures (MBT') show several degrees of temperature decline, following the summer insolation changes (Fig. 5). This temperature trend is consistent with the Zagoskin temperature record, and loss on ignition (overall productivity) data from Burial Lake, albeit they differ from chironomid-inferred temperatures from Burial Lake.

Another suite of bone samples was analyzed from sites excavated at Cape Krusenstern, on the Chukchi Sea coast, north of Kotzebue, Alaska. These samples show a slightly lower MBT'/CBT inferred temperature during the Little Ice Age, and are consistent with published reconstructions (McKay and Kaufman, 2014; Wiles et al., 2014) (Fig. 6; Figure S4). Interestingly, however, bones from marine sources consistently show slightly higher temperatures than those from terrestrial animals. The exact causes of these differences are unknown but based on the data from different bone sections, a likely cause is that variations

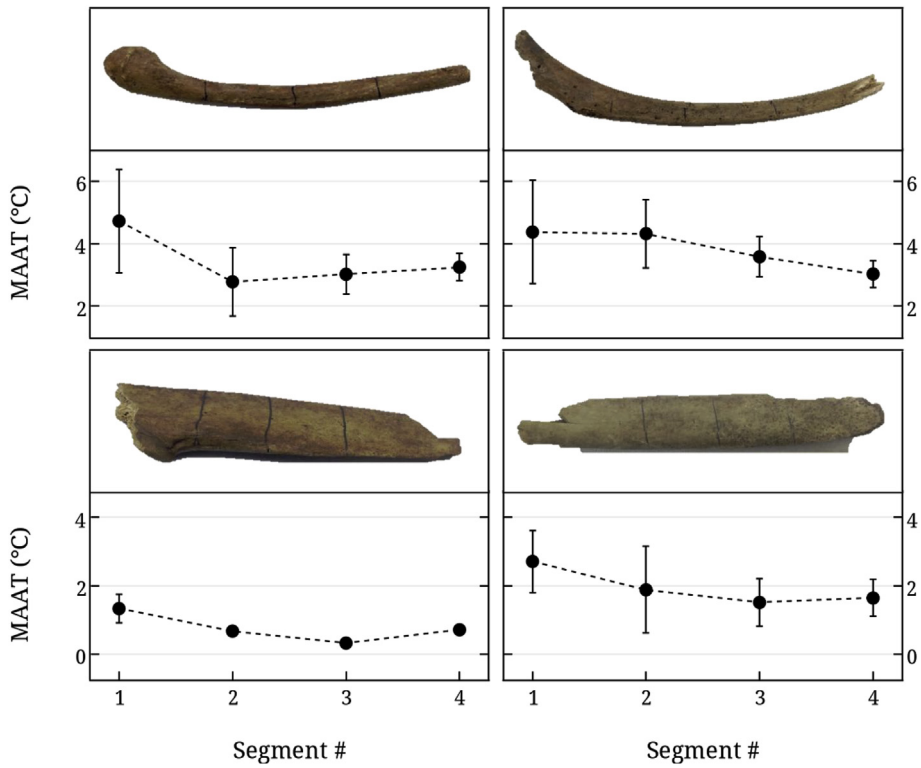

Fig. 7. Reconstructed temperatures using MBT'-CBT index from bone derived branched-GDGTs across different sections of selected long limb bones. MBT'/CBT calibration is used here (Peterse et al., 2012).

in bone density result in different levels of activity among different populations of br-GDGT-producing bacterial communities. The compositions of marine and terrestrial mammal bones on which the bacteria populations feed may also differ, leading to variations in the br-GDGTs that they produce.

Overall, the initial data presented here indicate that br-GDGTs in ancient bones record relative changes in past temperatures. This is consistent with our hypothesis that the bones serve as shelters for the br-GDGTs produced by ancient bacteria, with far less potential contamination and mixing of signals which affects the application of this proxy in soils and sediments. There are certainly limitations of this method, discussed below, emphasizing the need for further study. Regardless, thus far, we still see good agreement with existing paleoclimate records and other proxies where available, demonstrating the potential of this method to reconstruct relative changes and its potential to provide *in situ* environmental and climatic data on a site and region-specific level, and on timescales of human occupation.

3.4. Other factors that could affect br-GDGT distributions in bones

We also systematically sampled two long bone fragments to determine if br-GDGT-inferred temperatures may vary within a single bone (Fig. 7). Interestingly, some variation of inferred temperatures was observed. In general, samples that were taken closer to the proximal and distal ends of bones, which tend to be comprised of less cortical and more trabecular bone, display slightly higher inferred temperatures (i.e. they contain br-GDGTs with fewer methyl branches). One possible explanation for this observation is that the denser cortical bone may require a longer time for the bacterial growth to stop and thus produces signatures that reflect annual mean temperatures, whereas bacterial growth in the spongy trabecular bone may reflect biases towards rapid microbial proliferation during warmer times.

4. Conclusion

Our results represent the first applications to bones and suggest that a key class of climate-sensitive bacterial lipid compounds, namely br-GDGTs, are abundantly produced, preserved, and accessible in archaeological animal bones. Results from samples obtained from the FAC decomposition research facility indicate that these br-GDGT lipids are produced *in situ* as bacteria degrade organic matter inside the bone, and reflect climatic conditions at the time of deposition of the bone.

Unlike soils, which are continuously subject to secondary deposition and contamination processes, animal bones provide a physical shelter that prevents or at least minimizes inputs of br-GDGTs from later sources, enabling bone br-GDGTs to preserve past climate conditions. The bacterial population that produces br-GDGTs in bones probably originates from those in soils, and calibration of br-GDGTs using recent bone samples should therefore allow a more accurate reconstruction of past temperatures using ancient bones.

We conclude that it is possible to extract paleoclimate information directly from archaeological sites and to address directly the dynamics between climate change and factors that impact life and well-being of past communities. The recovery of climatic data from archaeological bones also opens the possibility of using bones from the relatively numerous archaeological sites scattered across most regions to expand the basis upon which the paleoclimate records are built, and to increase the regional coverage of paleo-climatic data sets beyond the limitations imposed by the distribution of conventional paleoclimate archives. Incorporating the relatively high-precision chronological control found in the stratigraphy of many archaeological sites and br-GDGT signatures formed over periods of time shorter than a human generation can also contribute to high resolution paleoclimate studies.

Significance statement

With ever faster technological innovations, anthropogenic activities are exerting increasingly more powerful impacts on the Earth's climate and environments, which in turn will profoundly affect human societies. It is a time for reflection, rather than complacency, as wrong decisions made by humans equipped with more and more sophisticated technologies could lead to ever-larger catastrophes. Lessons about how past climate and environmental changes affected ancient human societies are particularly pertinent, as they serve as models for making long-term government policies. However, our ability to accurately account for the impact of past climate change on human societies are undermined by the lack of *in situ* archives of climate variability in archaeological sites. This study proposes a new approach to this problem.

Acknowledgements

Funding for this study was provided by a Research Seed Award from Brown University's Office of the Vice President for Research and by the Institute at Brown for Environment and Society. We would like to thank Heather Olson and the Public Archaeology Laboratory (Pawtucket, RI) for providing samples from the northeastern U.S., Patrick Druckenmiller and Julie Rousseau from the University of Alaska Fairbanks for samples from Alaska's North Slope, Barbara Montgomery and Tierra Right of Way Services (Tuscon, AZ) for samples from the Southwestern U.S., and Sean Norris and Paul Webb from TRC Solutions (Columbia, SC) for samples from the Southeastern U.S. We would like to thank the Haffenreffer Museum of Anthropology for providing samples from Cape Krusenstern and the Joukowsky Institute for Archaeology and the Ancient World for providing samples from their collections and College Hill excavations for preliminary testing. Finally, we thank the following Brown University undergraduate students for their tireless efforts processing the bone samples used in this study: Julia Deng, Jacob Douglas, Jimena Terrazas Lozano, Alok Panray, Paige Parsons, Jarunetr Sae-Lim, and Anna Stacy.

Appendix A. Supplementary data

Supplementary data related to this article can be found at http://dx.doi.org/10.1016/j.jas.2018.05.009.

References

Anderson, S., Freeburg, A., Fitzhugh, B., 2014. Cape Krusenstern societies. In: Smith, C. (Ed.), Encyclopedia of Global Archaeology. Springer-Verlag, New York, pp. 1124–1131.

Anderson, S.L., Freeburg, A.K., 2014. High latitude coastal settlement patterns: cape Krusenstern, Alaska. J. Isl. Coast. Archaeol. 9, 295–318. http://dx.doi.org/10.1080/15564894.2013.840873.

Behrensmeyer, A.K., 1978. Taphonomic and ecologic information from bone weathering. Paleobiology 4, 150–162.

Blaga, C.I., Reichart, G.J., Schouten, S., Lotter, A.F., Werne, J.P., Kosten, S., Mazzeo, N., Lacerot, G., Sinninghe Damsté, J.S., 2010. Branched glycerol dialkyl glycerol tetraethers in lake sediments: can they be used as temperature and pH proxies? Org. Geochem. 41, 1225–1234. http://dx.doi.org/10.1016/j.orggeochem.2010.07.002.

D'Andrea, W.J., Huang, Y., Fritz, S.C., Anderson, N.J., 2011. Abrupt Holocene climate change as an important factor for human migration in West Greenland. Proc. Natl. Acad. Sci. 108, 9765–9769. http://dx.doi.org/10.1073/pnas.1101708108.

Dang, X., Yang, H., Naafs, B.D.A., Pancost, R.D., Xie, S., 2016. Evidence of moisture control on the methylation of branched glycerol dialkyl glycerol tetraethers in semi-arid and arid soils. Geochim. Cosmochim. Acta 189, 24–36. http://dx.doi.org/10.1016/j.gca.2016.06.004.

De Jonge, C., Hopmans, E.C., Zell, C.I., Kim, J.H., Schouten, S., Sinninghe Damsté, J.S., 2014. Occurrence and abundance of 6-methyl branched glycerol dialkyl glycerol tetraethers in soils: implications for palaeoclimate reconstruction. Geochim. Cosmochim. Acta 141, 97–112. http://dx.doi.org/10.1016/j.gca.2016.03.038.

Dirghangi, S.S., Pagani, M., Hren, M.T., Tipple, B.J., 2013. Distribution of glycerol dialkyl glycerol tetraethers in soils from two environmental transects in the USA. Org. Geochem. 59, 49–60. http://dx.doi.org/10.1016/j.orggeochem.2013.03.009.

Finkenbinder, M.S., Abbott, M.B., Finney, B.P., Stoner, J.S., Dorfman, J.M., 2015. A multi-proxy reconstruction of environmental change spanning the last 37,000 years from Burial Lake, Arctic Alaska. Quat. Sci. Rev. 126, 227–241. http://dx.doi.org/10.1016/

j.quascirev.2015.08.031.
Gao, L., Nie, J., Clemens, S., Liu, W., Sun, J., Zech, R., Huang, Y., 2012. The importance of solar insolation on the temperature variations for the past 110kyr on the Chinese Loess Plateau. Palaeogeogr. Palaeoclimatol. Palaeoecol. 317–318, 128–133. http://dx.doi.org/10.1016/j.palaeo.2011.12.021.
Giddings, J.L., Anderson, D.D., 1986. Beach Ridge Archaeology of Cape Krusenstern: Eskimo and Pre-eskimo Settlements Around Kotzebue Sounds, Alaska. National Park Service, Publications in Archaeology 20, US Department of Inerior, Washington, DC.
Haug, G.H., Günther, D., Peterson, L.C., Sigman, D.M., Hughen, K.A., Aeschlimann, B., 2003. Climate and the collapse of Maya civilization. Science 299, 1731–1735. http://dx.doi.org/10.1126/science.1080444. (80-.).
Hodell, D.A., Curtis, J.H., Brenner, M., 1995. Possible role of climate in the collapse of Classic Maya civilization. Nature. http://dx.doi.org/10.1038/375391a0.
Hopmans, E.C., Schouten, S., Sinninghe Damsté, J.S., 2016. The effect of improved chromatography on GDGT-based palaeoproxies. Org. Geochem. 93, 1–6. http://dx.doi.org/10.1016/j.orggeochem.2015.12.006.
Hopmans, E.C., Weijers, J.W.H., Schefuß, E., Herfort, L., Sinninghe Damsté, J.S., Schouten, S., 2004. A novel proxy for terrestrial organic matter in sediments based on branched and isoprenoid tetraether lipids. Earth Planet Sci. Lett. 224, 107–116. http://dx.doi.org/10.1016/j.epsl.2004.05.012.
Kaufman, D.S., Ager, T.A., Anderson, N.J., Anderson, P.M., Andrews, J.T., Bartlein, P.J., Brubaker, L.B., Coats, L.L., Cwynar, L.C., Duvall, M.L., Dyke, A.S., Edwards, M.E., Eisner, W.R., Gajewski, K., Geirsdottir, A., Hu, F.S., Jennings, A.E., Kaplan, M.R., Kerwin, M.W., Lozhkin, A.V., MacDonald, G.M., Miller, G.H., Mock, C.J., Oswald, W.W., Otto-Bliesner, B.L., Porinchu, D.F., Ruhland, K., Smol, J.P., Steig, E.J., Wolfe, B.B., 2004. Holocene thermal maximum in the western Arctic (0-180W). Quat. Sci. Rev. 23, 529–560. http://dx.doi.org/10.1016/j.quascirev.2003.09.007.
Kennett, D.J., Breitenbach, S.F.M., Aquino, V.V., Asmerom, Y., Awe, J., Baldini, J.U.L., Bartlein, P., Culleton, B.J., Ebert, C., Jazwa, C., Macri, M.J., Marwan, N., Polyak, V., Prufer, K.M., Ridley, H.E., Sodemann, H., Winterhalder, B., Haug, G.H., 2012. Development and disintegration of Maya political systems in response to climate change. Science 338, 788–791. http://dx.doi.org/10.1126/science.1226299. (80-.).
Kurek, J., Cwynar, L.C., Ager, T.A., Abbott, M.B., Edwards, M.E., 2009. Late Quaternary paleoclimate of western Alaska inferred from fossil chironomids and its relation to vegetation histories. Quat. Sci. Rev. 28, 799–811. http://dx.doi.org/10.1016/j.quascirev.2008.12.001.
Loomis, S.E., Russell, J.M., Ladd, B., Street-Perrott, F.A., Sinninghe Damsté, J.S., 2012. Calibration and application of the branched GDGT temperature proxy on East African lake sediments. Earth Planet Sci. Lett. 357–358, 277–288. http://dx.doi.org/10.1016/j.epsl.2012.09.031.
Mann, D.H., Groves, P., Kunz, M.L., Reanier, R.E., Gaglioti, B.V., 2013. Ice-age megafauna in Arctic Alaska: extinction, invasion, survival. Quat. Sci. Rev. 70, 91–108. http://dx.doi.org/10.1016/j.quascirev.2013.03.015.
Mason, O.K., Ludwig, S.L., 1990. Resurrecting beach ridge archaeology: parallel depositional records from St. Lawrence Island and cape Krusenstern, western Alaska. Geoarchaeology 5, 349–373. http://dx.doi.org/10.1002/gea.3340050404.
McKay, N.P., Kaufman, D.S., 2014. An extended Arctic proxy temperature database for the past 2,000 years. Sci. Data 1 (140026), 1–10. http://dx.doi.org/10.1038/sdata.2014.26.
Medina-Elizalde, M., Burns, S.J., Lea, D.W., Asmerom, Y., von Gunten, L., Polyak, V., Vuille, M., Karmalkar, A., 2010. High resolution stalagmite climate record from the Yucatan Peninsula spanning the Maya terminal classic period. Earth Planet Sci. Lett. 298, 255–262. http://dx.doi.org/10.1016/j.epsl.2010.08.016.
Naafs, B.D.A., Gallego-Sala, A.V., Inglis, G.N., Pancost, R.D., 2017. Refining the global branched glycerol dialkyl glycerol tetraether (brGDGT) soil temperature calibration. Org. Geochem. 106, 48–56. http://dx.doi.org/10.1016/j.orggeochem.2017.01.009.
Peterse, F., Prins, M.A., Beets, C.J., Troelstra, S.R., Zheng, H., Gu, Z., Schouten, S., Damsté, J.S.S., 2011. Decoupled warming and monsoon precipitation in East Asia over the last deglaciation. Earth Planet Sci. Lett. 301, 256–264. http://dx.doi.org/10.1016/j.epsl.2010.11.010.
Peterse, F., van der Meer, J., Schouten, S., Weijers, J.W.H., Fierer, N., Jackson, R.B., Kim, J.H., Sinninghe Damsté, J.S., 2012. Revised calibration of the MBT-CBT paleotemperature proxy based on branched tetraether membrane lipids in surface soils. Geochim. Cosmochim. Acta 96, 215–229. http://dx.doi.org/10.1016/j.gca.2012.08.011.
Potts, R., 1998. Environmental hypotheses of hominin evolution. Am. J. Phys. Anthropol. 107, 93–136. http://dx.doi.org/10.1002/(SICI)1096-8644. (1998) 107:27 + < 93::AID-AJPA5 > 3.0.CO;2-X.
Scherer, A.K., Golden, C., 2014. Water in the west: chronology and collapse of the Western Maya river Kingdoms. In: Iannone, G. (Ed.), The Great Maya Droughts in Cultural Context. University Press of Colorado, Boulder, pp. 207–229. http://dx.doi.org/10.5876/9781607322801.c010.
Schouten, S., Huguet, C., Hopmans, E.C., Kienhuis, M.V.M., Sinninghe Damsté, J.S., 2007. Analytical methodology for TEX 86 paleothermometry by high-performance liquid chromatography/atmospheric pressure chemical ionization-mass spectrometry. Anal. Chem. 79, 2940–2944. http://dx.doi.org/10.1029/2004PA001110. This).
Shanahan, T.M., Hughen, K.A., Van Mooy, B.A.S., 2013. Temperature sensitivity of branched and isoprenoid GDGTs in Arctic lakes. Org. Geochem. 64, 119–128. http://dx.doi.org/10.1016/j.orggeochem.2013.09.010.
Sinninghe Damsté, J.S., Hopmans, E.C., Pancost, R.D., Schouten, S., Geenevasen, J.A.J., 2000. Newly discovered non-isoprenoid glycerol dialkyl glycerol tetraether lipids in sediments. Chem. Commun. 1683–1684. http://dx.doi.org/10.1039/b004517i.
Sinninghe Damsté, J.S., 2016. Spatial heterogeneity of sources of branched tetraethers in shelf systems: the geochemistry of tetraethers in the Berau River delta (Kalimantan, Indonesia). Geochim. Cosmochim. Acta 186, 13–31. http://dx.doi.org/10.1016/j.gca.2016.04.033.
Tierney, J.E., Schouten, S., Pitcher, A., Hopmans, E.C., Sinninghe Damsté, J.S., 2012. Core and intact polar glycerol dialkyl glycerol tetraethers (GDGTs) in Sand Pond, Warwick, Rhode Island (USA): insights into the origin of lacustrine GDGTs. Geochim. Cosmochim. Acta 77, 561–581. http://dx.doi.org/10.1016/j.gca.2011.10.018.
Webster, J.W., Brook, G.A., Railsback, L.B., Cheng, H., Edwards, R.L., Alexander, C., Reeder, P.P., 2007. Stalagmite evidence from Belize indicating significant droughts at the time of preclassic abandonment, the Maya Hiatus, and the classic Maya collapse. Palaeogeogr. Palaeoclimatol. Palaeoecol. 250, 1–17. http://dx.doi.org/10.1016/j.palaeo.2007.02.022.
Weijers, J.W.H., Schouten, S., Hopmans, E.C., Geenevasen, J.A.J., David, O.R.P., Coleman, J.M., Pancost, R.D., Sinninghe Damsté, J.S., 2006a. Membrane lipids of mesophilic anaerobic bacteria thriving in peats have typical archaeal traits. Environ. Microbiol. 8, 648–657. http://dx.doi.org/10.1111/j.1462-2920.2005.00941.x.
Weijers, J.W.H., Schouten, S., Spaargaren, O.C., Sinninghe Damsté, J.S., 2006b. Occurrence and distribution of tetraether membrane lipids in soils: implications for the use of the TEX86 proxy and the BIT index. Org. Geochem. 37, 1680–1693. http://dx.doi.org/10.1016/j.orggeochem.2006.07.018.
Weijers, J.W.H., Schouten, S., van den Donker, J.C., Hopmans, E.C., Sinninghe Damsté, J.S., 2007a. Environmental controls on bacterial tetraether membrane lipid distribution in soils. Geochim. Cosmochim. Acta 71, 703–713. http://dx.doi.org/10.1016/j.gca.2006.10.003.
Weijers, J.W.H., Schefuss, E., Schouten, S., Sinninghe Damsté, J.S., 2007b. Coupled thermal and hydrological evolution of Tropical Africa over the last deglaciation. Science 315, 1701–1704. http://dx.doi.org/10.1126/science.1138131.
Weijers, J.W.H., Wiesenberg, G.L.B., Bol, R., Hopmans, E.C., Pancost, R.D., 2010. Carbon isotopic composition of branched tetraether membrane lipids in soils suggest a rapid turnover and a heterotrophic life style of their source organism(s). Biogeosciences 7, 2959–2973.
Wiles, G.C., D'Arrigo, R.D., Barclay, D., Wilson, R.S., Jarvis, S.K., Vargo, L., Frank, D., 2014. Surface air temperature variability reconstructed with tree rings for the Gulf of Alaska over the past 1200 years. Holocene 24, 198–208. http://dx.doi.org/10.1177/0959683613516815.
Wu, X., Dong, H., Zhang, C.L., Liu, X., Hou, W., Zhang, J., Jiang, H., 2013. Evaluation of glycerol dialkyl glycerol tetraether proxies for reconstruction of the paleo-environment on the Qinghai-Tibetan Plateau. Org. Geochem. 61, 45–56. http://dx.doi.org/10.1016/j.orggeochem.2013.06.002.
Xie, S., Pancost, R.D., Chen, L., Evershed, R.P., Yang, H., Zhang, K., Huang, J., Xu, Y., 2012. Microbial lipid records of highly alkaline deposits and enhanced aridity associated with significant uplift of the Tibetan Plateau in the Late Miocene. Geology 40, 291–294. http://dx.doi.org/10.1130/G32570.1.
Yancheva, G., Nowaczyk, N.R., Mingram, J., Dulski, P., Schettler, G., Negendank, J.F.W., Liu, J., Sigman, D.M., Peterson, L.C., Haug, G.H., 2007. Influence of the intertropical convergence zone on the East Asian monsoon. Nature 445, 74–77. http://dx.doi.org/10.1038/nature05431.
Yang, H., Pancost, R.D., Dang, X., Zhou, X., Evershed, R.P., Xiao, G., Tang, C., Gao, L., Guo, Z., Xie, S., 2014. Correlations between microbial tetraether lipids and environmental variables in Chinese soils: optimizing the paleo-reconstructions in semi-arid and arid regions. Geochim. Cosmochim. Acta 126, 49–69. http://dx.doi.org/10.1016/j.gca.2013.10.041.
Zhang, P., Cheng, H., Edwards, R.L., Chen, F., Wang, Y., Yang, X., Liu, J., Tan, M., Wang, X., Liu, J., An, C., Dai, Z., Zhou, J., Zhang, D., Jia, J., Jin, L., Johnson, K.R., 2008. A test of climate, sun, and culture relationships from an 1810-year Chinese cave record. Science 322, 940–942. http://dx.doi.org/10.1126/science.1163965. (80-.).
Zheng, Y., Li, Q., Wang, Z., Naafs, B.D.A., Yu, X., Pancost, R.D., 2015. Peatland GDGT records of Holocene climatic and biogeochemical responses to the Asian Monsoon. Org. Geochem. 87, 86–95. http://dx.doi.org/10.1016/j.orggeochem.2015.07.012.